www.acsnano.org

Tunable Orientation and Assembly of Polymer-Grafted Nanocubes at Fluid—Fluid Interfaces

Yilong Zhou, Tsung-Yeh Tang, Brian Hyun-jong Lee, and Gaurav Arya*



Downloaded via UNIV OF CALIFORNIA SAN DIEGO on April 22, 2022 at 19:37:15 (UTC). See https://pubs.acs.org/sharingguidelines for options on how to legitimately share published articles.

Cite This: https://doi.org/10.1021/acsnano.1c10416



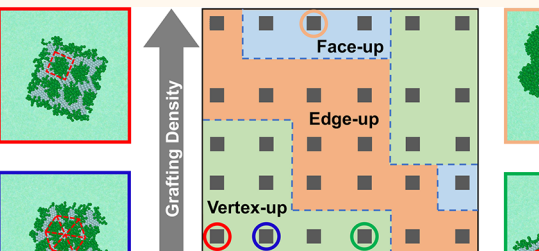
ACCESS

Metrics & More

Article Recommendations

s Supporting Information

ABSTRACT: Self-assembly of faceted nanoparticles is a promising route for fabricating nanomaterials; however, achieving low-dimensional assemblies of particles with tunable orientations is challenging. Here, we demonstrate that trapping surface-functionalized faceted nanoparticles at fluid—fluid interfaces is a viable approach for controlling particle orientation and facilitating their assembly into unique one-and two-dimensional superstructures. Using molecular dynamics simulations of polymer-grafted nanocubes in a polymer bilayer along with a particle-orientation classification method we developed, we show that the nanocubes can be induced into face-up, edge-up, or vertex-up orientations by tuning the graft



Vertex-up



density and differences in their miscibility with the two polymer layers. The orientational preference of the nanocubes is found to be governed by an interplay between the interfacial area occluded by the particle, the difference in interactions of the grafts with the two layers, and the stretching and intercalation of grafts at the interface. The resulting orientationally constrained nanocubes are then shown to assemble into a variety of unusual architectures, such as rectilinear strings, close-packed sheets, bilayer ribbons, and perforated sheets, which are difficult to obtain using other assembly methods. Our work thus demonstrates a versatile strategy for assembling freestanding arrays of faceted nanoparticles with possible applications in plasmonics, optics, catalysis, and membranes, where precise control over particle orientation and position is required.

KEYWORDS: faceted nanoparticles, nanoparticle assembly, surface tension, fluid—fluid interface, polymer grafting, nanoparticle strings, nanoparticle sheets

aceted nanoparticles (NPs) are appealing building blocks for fabricating materials due to their potential to self-assemble into unique architectures that cannot be accessed through assembly of spherical NPs. 1-4 Additionally, the presence of proximally adjacent edges, vertices, and flat surfaces in assemblies of faceted NPs invokes novel lightmatter interactions and catalytic properties that can be harnessed for various applications. 5-10 Thus, significant effort has gone into devising methods for synthesizing faceted NPs, 11,12 and a plethora of particle geometries ranging from simple cubes to more complex polyhedra are now routinely synthesized in laboratories. ^{4,13-15} Achieving NP assemblies of arbitrary rotational and translational order however remains a daunting task, 16,17 as conventional bulk assembly conditions generally lead to 3D close-packed arrangement of NPs representing their native minimum-free-energy configuration. 18 Various assembly strategies, mostly in the context of spherical NPs, have been proposed to achieve lower dimensional structures such as clusters, linear arrays, or sheets. 19 Briefly,

these approaches involve using polymer, ²⁰ DNA origami, ²¹ or surface templates to direct the placement of NPs; ²² functionalizing NPs in a patchy manner to control their coordination number; ²³ employing external fields ²⁴ and flows ²⁵ to assemble NPs into chains; and grafting NPs with polymers to introduce multibody interactions between NPs that favor low-dimensional assemblies. ^{19,26}

Recently, we proposed a promising strategy for assembling spherical NPs into unique clusters, strings, and sheets.²⁷ The approach involves using two mutually immiscible fluids to trap NPs at the interface formed between the fluids. Depending on

Received: November 23, 2021 Accepted: April 19, 2022



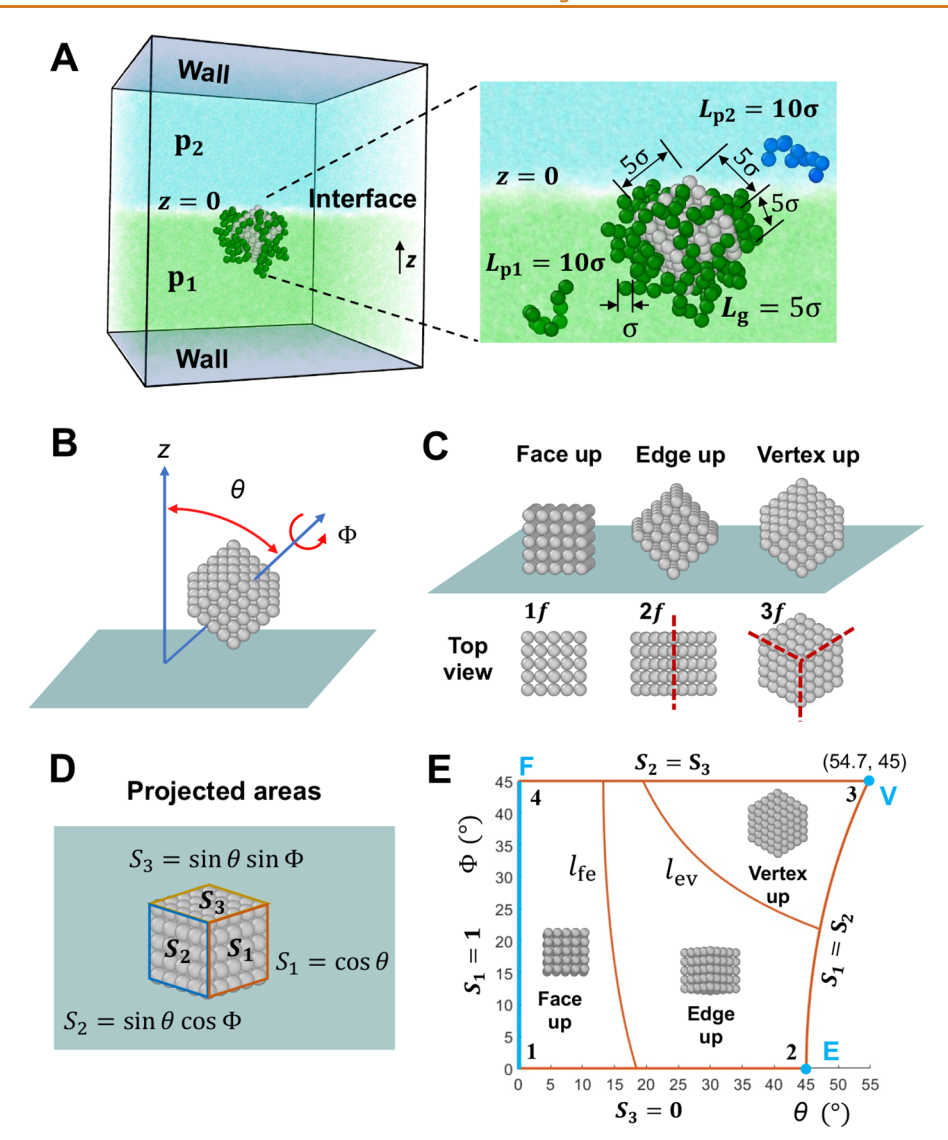


Figure 1. Simulation setup and orientation classification method. (A) Coarse-grained model of the polymer bilayer and polymer-grafted nanocubes. Throughout this study, the top and bottom polymer layers are shown in cyan and fluorescent green, the grafts selective to the bottom layer are shown in green (blue if top layer), and the nanocube cores are shown as cubic lattices of gray beads. (B) Angles θ and Φ used for describing the interfacial orientation of nanocubes. (C) Three principal orientations exhibited by interface-trapped nanocubes and their top views illustrating how their interface-projected area is dominated by one, two, and three faces. (D) Interface-projected areas S_1 , S_2 , and S_3 of the three faces (normalized by the area of a face) of a randomly oriented nanocube can be directly related to angles θ and Φ . (E) Due to symmetry, all possible orientations of a nanocube can be mapped onto a nondegenerate $\theta-\Phi$ space enclosed by four boundaries (shown in orange): $\Phi = 0^{\circ}$ ($S_3 = 0$), $\Phi = 45^{\circ}$ ($S_2 = S_3$), $\theta = 0^{\circ}$ ($S_1 = 1$), and $\tan \theta = 1/\cos \Phi$ ($S_1 = S_2$). The internal boundaries I_{fe} and I_{ev} given by $\tan \theta = 1/(3 \sin \Phi + 3 \cos \Phi)$ and $\tan \theta = 1/(5 \sin \Phi - \cos \Phi)$ are used for classifying nanocubes into face-up, edge-up, and vertex-up orientations. Pure face-up (F), edge-up (E), and vertex-up (V) orientations are shown by the blue line and dots.

whether the NPs interact similarly or differently with the two fluid layers, the NPs would get trapped at the interfacial plane or at a plane parallel but slightly displaced from it. However, such interface-trapped NPs, if sufficiently attractive to each other, would simply assemble into a free-floating hexagonally packed monolayer to maximize interparticle contacts, a well-studied assembly outcome. ^{28–30} To overcome this limitation and achieve more unique assemblies, we proposed *co-assembly* of multiple species of NPs, each species trapped in a distinct plane at or near the interfacial plane based on how the NP interacts with the two fluids. We showed that the displacement direction of the planes can be controlled by grafting the NP surface with polymer chains that are preferentially miscible with one of the fluids, and the extent of displacement can be precisely tuned by varying the grafting density. By exploiting

the competition between interfacial forces, which attempt to trap NPs at their preferred locations at or near the interface, and interparticle forces, which attempt to maximize the number of contacts between NPs, we were able to achieve unique 2D bilayer assemblies from two species of NPs. By further harnessing multibody effects arising from steric interactions of the polymer grafts, we were able to demonstrate the assembly of unique clusters and quasi-1D architectures such as serpentine strings and networks.

The success of this approach naturally raises a question about its potential to assemble anisotropic particles such as the faceted NPs introduced above, which possess rotational degrees of freedom in addition to translation. We recall that the reason that a spherical NP that is "neutral" to both fluids positions itself symmetrically about the interfacial plane is

because this position maximizes the interfacial area occluded by the particle, providing the largest reduction in free energy of the interface. ^{30,31} For a neutral anisotropic NP, the interface should then be able to not only position but also orient the particle to maximize its cross-sectional area with the interfacial plane.³² Consider, for example, a neutral nanocube that can exhibit three possible idealized orientations at the interface: face-up, edge-up, or vertex-up. 32,33 Based on the interfacial area occluded by each orientation for a particle symmetrically positioned at the interfacial plane, the nanocube should prefer the edge-up orientation, which occludes the largest area, followed by the vertex-up and then the face-up orientation with the smallest area.³³ While this appears straightforward, what orientation a polymer-grafted nanocube would adopt is not so obvious, especially one grafted with chains selective to one of the fluids. The reason is that such chains would displace the nanocube away from the interfacial plane so that the area occluded by the three orientations no longer needs to follow the above sequence. Furthermore, the grafted chains will point in distinct directions as they emerge from the NP facets, possibly leading to different interactions with the interface for each orientation. This hypothesized ability of polymer grafting to tune the orientation of anisotropic NPs raises the intriguing possibility of controlling their subsequent assembly.³⁴ The different particle orientations should lead to fundamentally different interactions between them that combined with steric and multibody effects 19,26 of the polymer grafts has the potential to lead to new and emergent assembly morphologies.27

Here, we investigate through molecular dynamics (MD) simulations this hypothesized role of polymer grafts in governing the orientation and assembly behavior of interfacetrapped faceted NPs, using polymer-grafted nanocubes trapped at the interface formed between two mutually immiscible polymer melts as our model system. Our simulations show that compared to bare nanocubes that exhibit a single orientation at the interface, the polymer-grafted nanocubes can exhibit all three types of orientations depending on the grafting density and relative miscibility of the grafts with the two polymer layers. We further demonstrate how these different varieties of orientationally locked nanocubes can assemble into unique 1D and 2D higher-order architectures that cannot be achieved by bulk assembly of faceted NPs or by interfacial assembly of spherical ones. Thus, the assembly approach proposed here could be used to fabricate unique NP assemblies with possible applications in plasmonics, optics, membranes, and catalysis, where control over particle orientations and positions is required.

RESULTS AND DISCUSSION

Model Overview. We used MD simulations to investigate the orientation and assembly of polymer-grafted nanocubes in a bilayer formed by two mutually immiscible polymers. Nanocubes were chosen as our model particle because they have the potential to assemble into diverse superstructures through different types of interparticle contacts, *via* edges, vertices, and faces. Also, nanocubes can be easily synthesized, and previous work has shown that even simple assemblies of nanocubes made of iron, silver, and cesium oxide can exhibit unique properties, such as stabilized magnetization, optical absorption, and oxidation catalysis, respectively. A polymer-based interface was chosen to be consistent with our earlier

We adopted a coarse-grained model to describe the polymer-grafted nanocubes and polymer bilayer (Figure 1A; see Methods for details). Briefly, the polymer grafts ("g") and the bilayer polymers ("p1" and "p2") were treated as flexible bead-chains of lengths $L_g = 5$ and $L_{p1} = L_{p2} = 10$ beads, where each bead represents a short segment of the polymer chain.³⁷ We assumed that polymer chains of the same type were fully miscible with each other, the two polymers making up the bilayer were mutually immiscible, and the grafts were fully miscible with one polymer layer (p₁) and miscible to varying extents with the other layer. The miscible p_1-p_1 , p_2-p_2 , g-g, and g-p₁ intersegment interactions were modeled using a potential that accounts for both excluded volume and attractive interactions, with parameters σ and ε specifying the size and attraction strength of the segments, which also set the length and energy scales of the system. The variably miscible $g-p_2$ interactions were also treated using a similar potential of size parameter σ but adjustable attraction strength $\lambda \varepsilon$. The immiscible p₁-p₂ interactions were treated using a shortrange repulsive potential of size parameter σ that accounts for excluded-volume interactions. The nanocubes ("n") were modeled as rigid 5 \times 5 \times 5 lattices of beads, also of size σ , representing groups of lattice atoms. For convenience, the nanocubes were assumed to be immiscible with all polymer chains, and the nanocube beads interacted with beads on other nanocubes with a potential of attraction strength ε_n . We explored λ values in the range 0.1 to 1 representing nearly immiscible to fully miscible grafts, grafting densities Γ of 0.16 to 1.0 chains/ σ^2 representing mushroom to weak-brush regimes, and nanocube interbead attraction strengths $\varepsilon_{\rm n}$ of $0.5-2.5\varepsilon$. All MD simulations were carried out in the canonical ensemble at a temperature of $T = \varepsilon/k_B$ (k_B : Boltzmann constant) and a segment density of 0.85 beads/ σ^3 , which produces a melt-like state of the bilayer.

This minimalistic model captures the essential physics of interfacial NP-polymer systems while allowing access to the large length and time scales required for studying dynamics and assembly of polymer-grafted NPs. In particular, the model accounts for interfacial tension and thermal fluctuations of the polymer bilayer; conformational properties of free *versus* tethered chains including their entropy; differences in graft interactions with the two layers; van der Waals (vdW) and steric interactions between NPs; and all shape-associated effects of the nanocubes. 34,38-41

Classification of Particle Orientations. To characterize the behavior of nanocubes trapped at the interface, we developed a computational approach for classifying particle orientations from simulation trajectories. Since the orientations being examined are with respect to a 2D interface, only two rotational degrees of freedom are needed to fully describe orientation: a polar angle θ between the interface normal vector and the particle's internal "vertical" axis and an internal Euler angle Φ describing the particle's rotation about its own vertical axis ⁴² (Figure 1B). Our approach determines θ and Φ for the simulated nanocube configurations and classifies their orientation into one of the three principal orientations: faceup, edge-up, or vertex-up.

The underlying basis of this approach is that the interfaceprojected area of a nanocube is dominated by different numbers of faces in the three orientations: a *single* face contributes the entire projected area in pure face-up

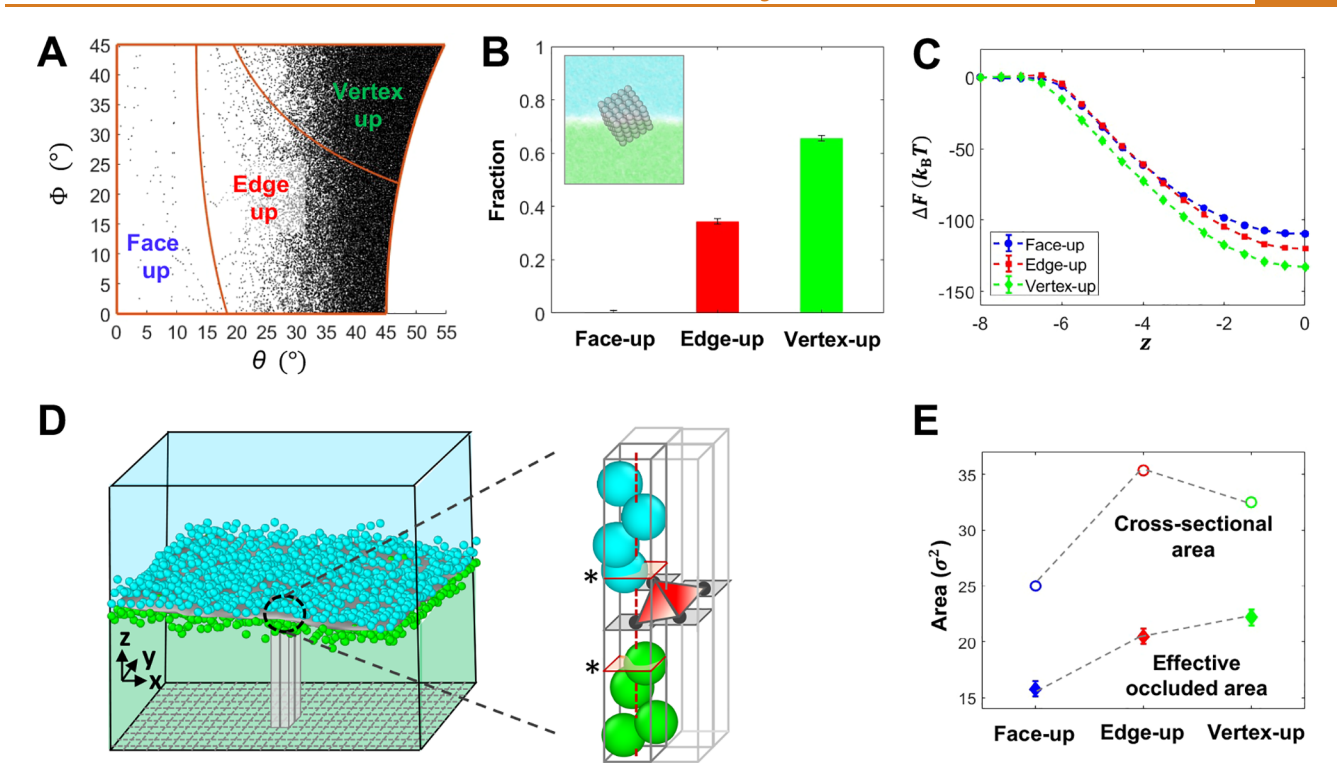


Figure 2. Orientational behavior of bare nanocubes at an interface. (A) Orientation angles sampled (black dots) by the nanocube in an MD simulation. (B) Fraction of nanocubes exhibiting the three principal orientations calculated from the angle distribution in (A). Inset: Representative snapshot of the nanocube in a bilayer captured from the simulation. (C) Free energy profiles $\Delta F(z)$ of nanocubes constrained in pure face-up, edge-up, and vertex-up orientations as a function of their position z from the interfacial plane. (D) Schematic of the triangulation scheme used for determining the surface area of the undulating interface. The simulation box is divided into $M \times N$ cells in the xy plane. The shape of the interface is determined by locating the midpoints (black dots in inset) of the closest pair of polymer beads (marked by an asterisk) of the top and bottom layers in each such cell. The total area of the interface is calculated as the sum of the areas of the triangular elements (shown in red) formed by all such MN midpoints. (E) Interfacial area occluded by nanocubes sitting in pure face-up, edge-up, and vertex-up orientations compared against their cross-sectional areas in the three orientations assuming a flat interface.

orientation, while two and three faces account for all the projected area in pure edge-up and vertex-up orientations, respectively (Figure 1C). Since all other orientations can be viewed as perturbations of these three orientations, arbitrarily oriented nanocubes can be classified into one of these orientations based on how similar area contributions of their three faces resemble those in the pure forms of these orientations. Specifically, an orientation is classified as face-up if the fraction of projected area contributed by its "dominant" face (the one contributing the largest area) is between 3/4 and 1; the critical value of 3/4 here was obtained as the midpoint of the fractions 1/2 and 1 contributed by the dominant face in the pure edge-up and face-up orientations, respectively. Otherwise, the orientation is categorized as edge-up if the fraction of the projected area contributed by the top-two dominant faces is between 5/6 and 1, where the value of 5/6 was obtained as the midpoint of the area fractions 2/3 and 1 contributed by the two most dominant faces in pure vertex-up and edge-up orientations. If both these conditions are not satisfied, the orientation is classified as vertex-up.

Since the interface-projected areas of the three faces (normalized by the area of a face) are related to the orientation angles via $S_1 = \cos \theta$, $S_2 = \sin \theta \cos \Phi$, and $S_3 = \sin \theta \sin \Phi$ (Figure 1D), the classification criteria introduced above can be mapped onto the orientation space (θ, Φ) . Furthermore, by recognizing that the faces of a cube are indistinguishable and have 4-fold symmetry and that θ and Φ can be defined based on $S_1 \geq S_2 \geq S_3$ without any loss of

generality (Figure S1), the entire orientation space $\theta \in [0^\circ, 180^\circ]$ and $\Phi \in [0^\circ, 360^\circ]$, which has high degeneracy, can be reduced to a much smaller, nondegenerate region bounded by $\Phi = 0^\circ$, $\Phi = 45^\circ$ ($S_2 = S_3$), $\theta = 0^\circ$, and $\tan \theta = 1/\cos \Phi$ ($S_1 = S_2$) (Figure 1E). This $\{S_1, S_2, S_3\} \rightarrow \{\theta, \Phi\}$ mapping yields the following bounds for the three orientations (see Methods for derivation):

face-up:

$$0 \le \theta < \tan^{-1}[1/(3\sin\Phi + 3\cos\Phi)]$$
 $0^{\circ} \le \Phi \le 45^{\circ}$

edge-up:

$$\tan^{-1}[1/(3\sin\Phi + 3\cos\Phi)] \le \theta \le \tan^{-1}[1/\cos\Phi]$$

 $0^{\circ} \le \Phi \le 21.8^{\circ}$

$$\tan^{-1}[1/(3\sin\Phi + 3\cos\Phi)] \le \theta$$

 $\le \tan^{-1}[1/(5\sin\Phi - \cos\Phi)] \quad 21.8^{\circ} < \Phi \le 45^{\circ}$

vertex-up:

$$\tan^{-1}[1/(5\sin\Phi - \cos\Phi)] < \theta \le \tan^{-1}[1/\cos\Phi]$$

21.8° < Φ < 45°

where the *pure* face-up $(S_1 = 1, S_2 = S_3 = 0)$, edge-up $(S_1 = S_2, S_3 = 0)$, and vertex-up $(S_1 = S_2 = S_3)$ orientations are specified by $(\theta, \Phi) = (0^\circ, [0^\circ, 45^\circ])$, $(45^\circ, 0^\circ)$, and $(54.7^\circ, 45^\circ)$, respectively.

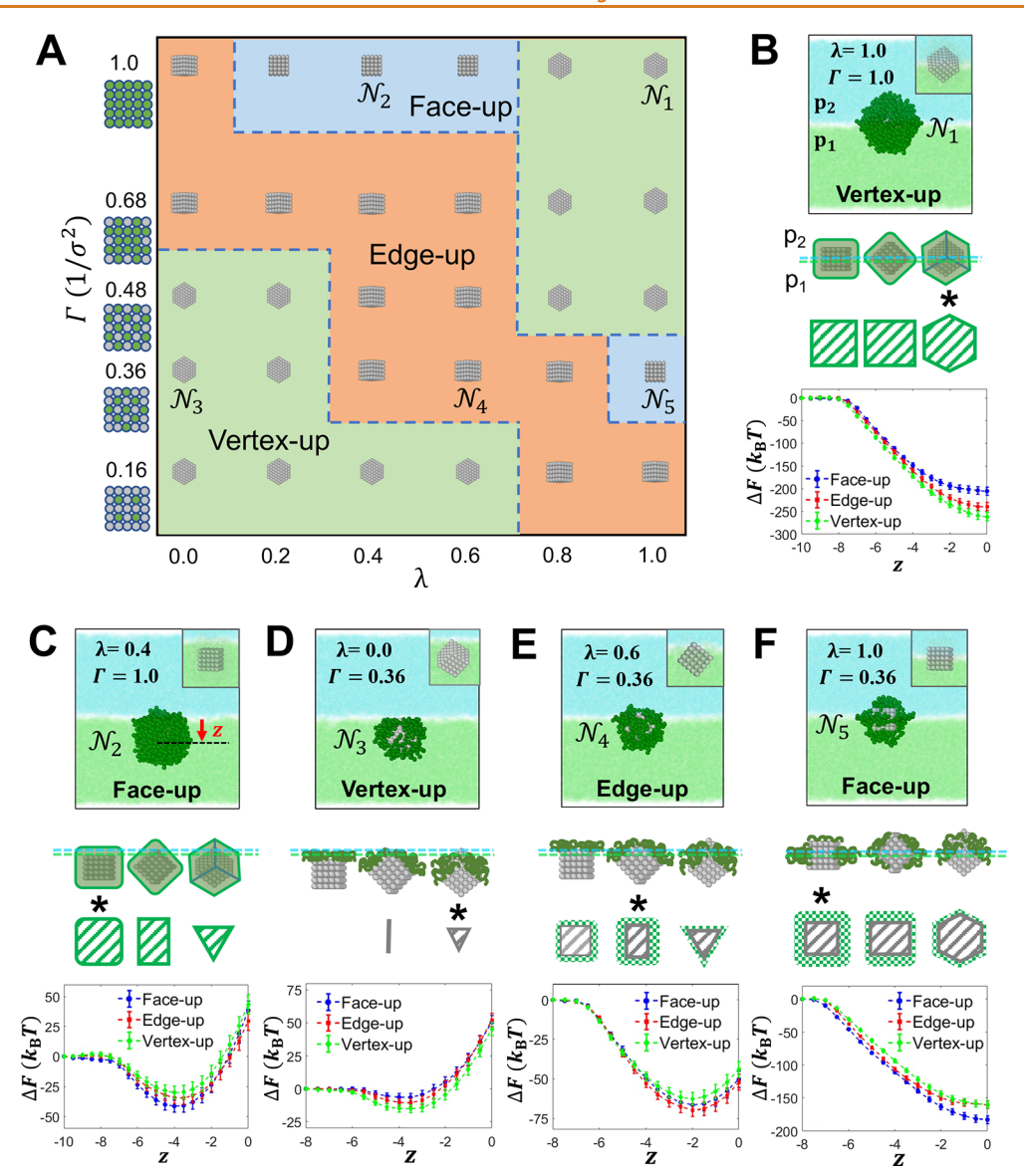


Figure 3. Orientational behavior of polymer-grafted nanocubes at an interface. (A) Phase diagram showing orientation preference of such nanocubes as a function of grafting density Γ (graft attachment points on the nanocube surface at each Γ are shown by green circles) and relative miscibility λ . (B–F) Analyses carried out to elucidate the orientational behavior of the representative nanocubes labeled $\mathcal{N}_1 - \mathcal{N}_5$ in the phase diagram. Top: Snapshot of nanocube captured from MD simulations (insets show nanocube orientations more clearly without their grafts). Middle: Schematic of interface-trapped nanocubes and the interfacial area they would occlude in each orientation (asterisk indicates orientation with largest occluded area). See Figure 4 and Figure S7 for complete analysis. Densely grafted nanocubes (B and C) can be treated as larger versions of their cubic cores, while the grafts and cubic cores need to be treated separately in sparsely grafted nanocubes (D–F). Bottom: Free energy profiles $\Delta F(z)$ of the nanocubes constrained in pure face-up, edge-up, and vertex-up orientations as a function of their position z from the interfacial plane.

Orientation of Bare Nanocubes. As a first step to understanding the behavior of polymer-grafted nanocubes, we carried out equilibrium MD simulations of a *bare* nanocube immersed in a polymer bilayer. As expected, the nanocube symmetrically straddled the interfacial plane (Figure 2B, inset); the particle is equally miscible with both polymer layers in our model, so this position leads to the largest reduction in interfacial area between the two polymers. To study the orientational behavior of the nanocube, we plotted the θ and Φ angles sampled during the simulation onto the orientation classification map introduced above (Figure 2A). The data show that the nanocube fluctuates mostly between the edge-up and vertex-up states. To characterize the orientation preference more quantitatively, we determined from the sampled angles

the fraction of nanocube configurations exhibiting the three orientations. The vertex-up orientation was found to be the preferred orientation (fraction $\sim 2/3$), followed by the edge-up orientation (fraction $\sim 1/3$), while the face-up orientation occurs rarely (Figure 2B; also see Figure S2A).

This result was further confirmed through free energy calculations. We held the nanocube in pure face-up, edge-up, and vertex-up orientations and computed for each of the three cases the free energy $\Delta F(z)$ of the system as a function of nanocube position z from the interfacial plane relative to the free energy where the nanocubes are located far from the interface. The computed free energy profiles for the three cases (Figure 2C) show that the vertex-up orientation provides the largest gain in free energy at the interfacial plane (i.e., the

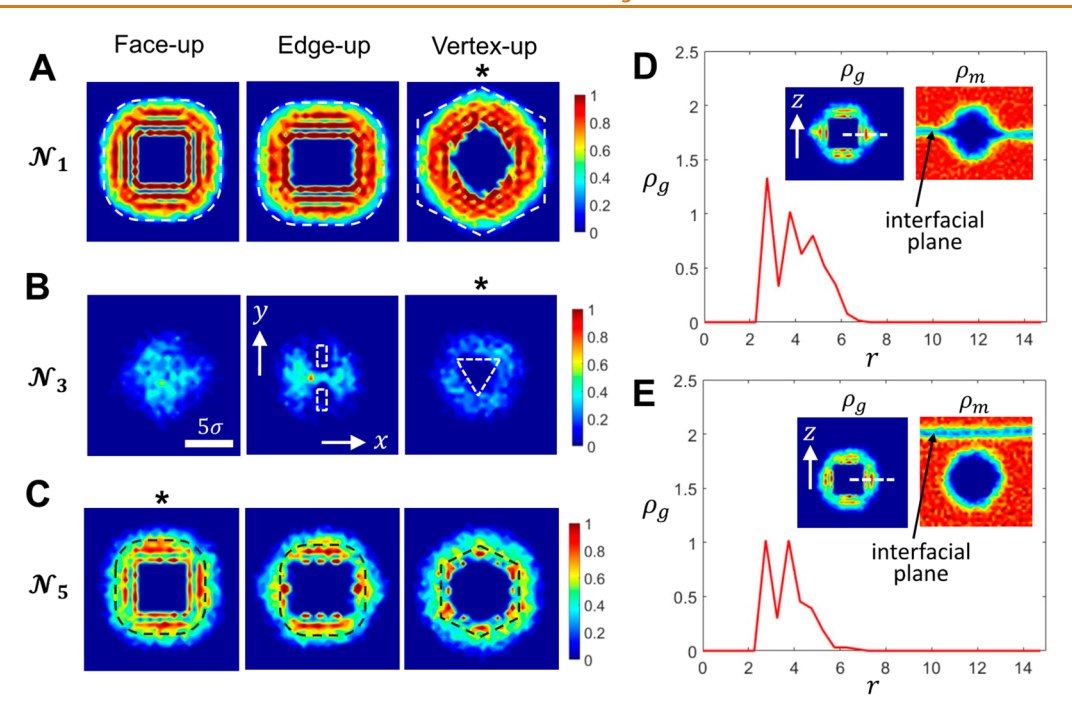


Figure 4. Analyses of polymer segment density around nanocubes. (A–C) Contour map of the segment density contributed by grafts around nanocubes along the interfacial plane. Results are plotted for nanocubes \mathcal{N}_1 (A), \mathcal{N}_3 (B), and \mathcal{N}_5 (C) constrained to face-up, edge-up, and vertex-up orientations and their corresponding equilibrium (minimum ΔF) positions z normal to the interface. The occluded interfacial areas are roughly shown enclosed by dashed lines, and the orientation with the largest occluded area is indicated by an asterisk. (D, E) Graft segment density surrounding nanocube \mathcal{N}_5 at the interface (D) and in bulk (E) as a function of distance from the nanocube center (along the dashed line shown in the inset). Insets show the contour map of graft-contributed segment density $\rho_{\rm m}$ perpendicular to the interfacial plane. All densities are in units of polymer beads/ σ^3 .

largest $|\Delta F(0)|$ value) followed by the edge-up and then the face-up orientation, consistent with the order of orientation preference observed in our simulations. Interestingly, all three orientations yielded large $|\Delta F(0)|$ (>100 $k_{\rm B}T$), highlighting the strength with which fluid—fluid interfaces trap NPs.

Our finding that symmetrically trapped nanocubes favor the vertex-up orientation seems to go against geometric arguments, 33 which suggest that the pure edge-up orientation should be the favored orientation, as it occludes a larger area of the interface ($\approx 1.414a^2$, where a is the nanocube side length) compared to the pure vertex-up ($\approx 1.299a^2$) and face-up orientations (a^2) (Figure S2B). This disagreement may be attributed to deformations of the interface: both large-scale modulations caused by the trapped particle and molecularscale fluctuations that effectively give a finite thickness to the interface 42,43 (Figure S3). Both these effects are ignored in these geometric arguments that view the interface as a perfectly flat plane of zero thickness. The true interfacial area occluded by the nanocube could therefore deviate from the above predictions to potentially change the order in which the three orientations are favored. To test this hypothesis, we analyzed the true instantaneous shape of the interface from equilibrium MD simulations of the polymer bilayer with the nanocube restrained at the interfacial plane in the three different pure orientations and without the nanocube. Using a surface triangulation scheme that accounts for both large- and smallscale interface deformations (Figure 2D, also see Methods), we computed the average area of the interface with and without the nanocube, as denoted by A'_1 and $A_{\rm I}$, which were used for calculating the average occluded area $\Delta A = A_{\rm I} - A'_{1}$. The ΔA for the three specific orientations are shown in Figure 2E, and indeed, the vertex-up orientation, and not the edge-up

orientation as predicted by geometry, is found to occlude the largest interfacial area. Moreover, the occluded areas for all three orientations follow the sequence predicted by our simulations and free energy calculations. Interestingly, these areas are also smaller than those predicted by geometry assuming a flat interface, further supporting the interface deformation hypothesis. Our results are also in good agreement with previously proposed continuum models that predicted the vertex-up orientation as the favored orientation of an interface-trapped cube when capillary effects and nonzero thickness of the interface were taken into account, ^{42,43} and neglecting capillarity led to the wrong orientation (edge-up) being favored.⁴²

Orientational Phase Diagram of Polymer-Grafted Nanocubes. We next studied how the orientation of a nanocube might be modulated by grafting polymer chains onto its surface. On the basis of our previous study on spherical NPs, we would expect grafting to shift the equilibrium position of the nanocubes away from the interfacial plane when the grafts have different miscibility with the two polymer layers of the bilayer. Indeed, MD simulations of freely mobile nanocubes grafted with chains fully miscible with one layer and partially miscible with the other show that increasing the grafting density Γ of the chains while keeping their relative miscibility λ (<1) fixed, or alternatively decreasing their relative miscibility difference λ while keeping Γ fixed, causes the average position z of the nanocubes to shift away from the interfacial plane and toward the layer more compatible with the grafted chains (Figure S4A and B). By the same principle, polymer grafting should also be able to modulate the equilibrium orientation of nanocubes, as they would attempt to orient in a manner that maximizes the area of the interface

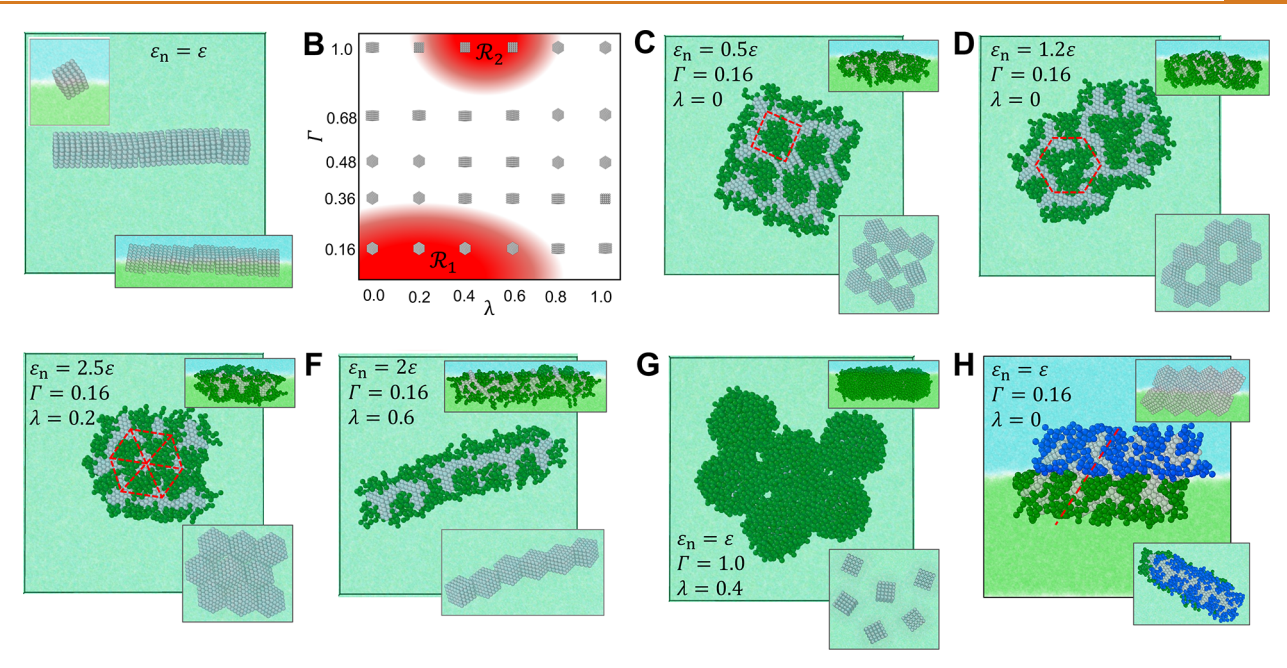


Figure 5. Higher-order structures of nanocubes assembled at the interface. (A) Linear string with face—face contacts assembled from bare nanocubes. Inset: Single nanocube exhibiting vertex-up orientation (top) and assembled structure with edge-up nanocubes (bottom) seen from a view parallel to the interface. (B) Orientational phase diagram showing regions \mathcal{R}_1 and \mathcal{R}_2 (shaded red) of the Γ - λ parameter space where polymer-grafted nanocubes (large $\varepsilon_n = 2.5\varepsilon$) display a tendency to self-assemble. (C-F) Assembly structures obtained from sparsely grafted nanocubes: perforated square-ordered monolayer (C), perforated hexagonally ordered monolayer (D), hexagonally close-packed monolayer (E), and linear string (F). The nanocubes retain their vertex-up orientation in all structures. (G) Hexagonally close-packed monolayer of face-up nanocubes obtained from assembly of densely grafted nanocubes. Inset: Structures seen from a view parallel to the interface (top) and structures without their grafts for better visualization (bottom). (H) Linear ribbon obtained from coassembly of two antisymmetric species of polymer-grafted nanocubes. Inset: Structure without grafts for better visualization (top) and top view of the structure (bottom). Red dashed lines guide the eye to the underlying particle arrangement.

they occlude while minimizing unfavorable interactions between their grafts and the polymer layer less compatible with them. The final, preferred orientation of the nanocube should then be determined by the interplay between these two effects

To investigate how these two effects govern the orientation of polymer-grafted nanocubes, we determined from equilibrium MD simulations, via our orientation classification approach, the preferred orientation of nanocubes as a function of grafting density Γ and relative miscibility λ , two parameters that affected the z-position of the nanocubes and should thereby also affect their orientation (Figure S5). Figure 3A presents the orientational "phase" diagram collated from such orientations determined at various points in the $\Gamma - \lambda$ parameter space. The nanocubes exhibit a vertex-up orientation in two regions of the phase diagram: at low Γ and small λ , and at the diagonally opposite condition of high Γ and large λ . In between these two regions and along the other diagonal connecting high Γ -small λ and low Γ -large λ points, the nanocubes exhibit an edge-up orientation. The face-up orientation also occupies two regions of the diagram: one region at high Γ and intermediate λ , and a smaller region at intermediate Γ and large λ . The existence of all three orientations in the phase diagram demonstrates that polymer grafting is a viable approach for tuning the interfacial orientation of nanocubes and faceted NPs more generally.

Next, we attempted to understand the physics behind the peculiar shape of the obtained phase diagram by analyzing the equilibrium z-positions, graft conformations, occluded interface areas, and free energies of representative nanocube systems covering all relevant regions of the phase diagram.

We begin by examining the behavior of densely grafted nanocubes with $\Gamma = 1.0$ chains/ σ^2 labeled \mathcal{N}_1 and \mathcal{N}_2 in Figure 3A that exhibit the vertex-up and face-up orientations, respectively. The computed polymer segment density contributed by grafts in Figure 4A (see also Figure S7A and B, left) show the existence of a dense graft corona that blocks direct interactions between the nanocube core and the polymer matrix, as also confirmed by the near-zero NP core-matrix interaction free energy shown in Figure S7A and B, right. The graft corona thus retains the cubic shape of the underlying nanocube cores, and the particles simply appear as larger versions of their cubic cores (Figure 3B and C). Nanocube N_1 whose grafts are equally miscible with both p_1 and p_2 ($\lambda = 1$) therefore sits symmetrically at the interfacial plane (Figure 3B, top). Due to these attributes, this nanocube behaves similarly to the bare nanocubes studied earlier, exhibiting the same vertex-up orientation (Figure 3B, middle) that our earlier analyses showed to occlude the largest interfacial area, as also seen from Figure 4A. In contrast, N_2 interacts less favorably with p_2 ($\lambda = 0.4$), so the particle shifts away from the interfacial plane and into p₁ to avoid unfavorable interactions with p₂ (Figure 3C, top). As shown schematically (Figure 3C, middle) and confirmed by the computed graft segment density at the interface plane (Figure S7B), the face-up orientation allows such a nanocube to not only maximally occlude the interface but also minimally intrude into the less favored polymer layer, whereas the other two orientations would yield lesser occluded areas at the same particle position z or larger surface area of relatively unfavorable graft $-p_2$ interactions at smaller |z|. The computed free energy profiles $\Delta F(z)$ confirm that the vertexup and face-up orientations indeed yield the most favorable interfacial entrapment free energies (largest $|\Delta F(z)|$ at the minima) for \mathcal{N}_1 and \mathcal{N}_2 , respectively (Figure 3B and C, bottom).

The nanocubes grafted with chains at lower grafting densities $(N_3 - N_5)$ with $\Gamma = 0.36$ chains σ^2 need be analyzed slightly differently. Because the nanocube cores are more exposed here, interactions mediated by both the grafts and the cores become relevant (Figure S7C-E, right), different from \mathcal{N}_1 and \mathcal{N}_2 , where only graft-mediated interactions are important. Nanocube N_3 possesses grafts that are completely immiscible with p_2 ($\lambda = 0$), so the nanocube is pushed deep into p_1 (Figure 3D, top). Because N_3 is sparsely grafted, it adopts a vertex-up orientation that allows its grafts to completely avoid interacting with p2 while still allowing the nanocube core (Figure S7C, right), which is neutral to both layers, to occlude some interfacial area (Figure 3D, middle; Figure 4B). In contrast, nanocube N_4 attached with grafts of intermediate miscibility with p_2 ($\lambda = 0.6$) does not need to get pushed as deep into this layer as N_3 , providing the nanocube core opportunity to occlude more interfacial area (Figure 3E, top). Furthermore, as these grafts now interact more favorably with p_2 (compared to p_1-p_2 interactions), the graft chains stretch toward the interface (Figure S7D) to occlude the highly unfavorable p_1-p_2 interactions while gaining some favorable interactions with p₂ (Figure 3E, middle). In such situation where both the grafts and the nanocube cores contribute to occluded interfacial area, the edge-up orientation ends up occluding a larger area of the interface (Figure S7D, left) compared to the vertex-up orientation observed in N_3 . This stretching behavior of grafts becomes highly pronounced in nanocube N_5 , where the grafts are highly miscible with p_2 ($\lambda =$ 1). Here, the nanocube sits symmetrically at the interface due to equal miscibility of its grafts with p₁ and p₂. This chainstretching behavior is also observed in the computed 1D and 2D plots of the graft segment density along the interface (Figure 4D), which show conspicuous enhancement and spreading of density at the interface as compared to that obtained for nanocubes in the bulk (Figure 4E). Although the core of such a symmetrically positioned nanocube would occlude the largest interfacial area by adopting the vertex-up orientation, followed by the edge-up orientation (Figure 2A and E), the face-up orientation provides the best opportunity for the grafts to maximally stretch out toward the interface and intercalate into the gap between the two polymer layers (Figure 3F, top and middle), leading to overall larger occlusion of the interface compared to the other two orientations (Figure 4C). The free energy profiles verify that the vertex-up, edge-up, and face-up orientations indeed provide the largest energetic benefits for nanocubes $N_3 - N_5$ with sparser grafts (Figures 3D-F. bottom).

Assembly Behavior of Bare and Polymer-Grafted Nanocubes. Having shown that polymer grafting can be used to control the orientation of nanocubes at fluid—fluid interfaces, we next investigated how these nanocubes with different stabilized orientations assemble into higher-order structures. Starting with bare nanocubes, MD simulations of multiple such nanocubes in a polymer bilayer revealed that they assembled *via* face—face contacts into linear strings with edge-up orientations at the interface (Figure 5A), even though individually the nanocubes prefer being vertex-up at the interface (Figure 2A). Thus, even though reorientation of

nanocubes costs interfacial free energy $(\Delta F_{\rm E}(0) - \Delta F_{\rm V}(0) \approx +13k_{\rm B}T$ from Figure 2C, where subscripts E and V denote the edge-up and vertex-up states), it is more than compensated by the large free energy gained from face—face contacts $(\Delta F_{\rm FF} \approx -56k_{\rm B}T;$ Figure S8A). The alternative scenarios of nanocubes assembling *via* edge—edge contacts or them retaining their vertex-up orientation and assembling *via* tip-to-tip contacts are less favorable. These scenarios lead to much smaller contact free energies of $\Delta F_{\rm EE} \approx -7k_{\rm B}T$ (Figure S8B) and $\Delta F_{\rm VV} \approx -5k_{\rm B}T$ (Figure S8C) due to the significantly smaller surface area involved in such contacts.

To study the assembly of polymer-grafted nanocubes, the parameter space that needs to be explored is very large; relevant parameters include the grafting density Γ , graft relative miscibility λ , and nanocube-nanocube interaction strength ε_n . Therefore, we first roughly mapped out regions of the parameter space that permitted assembly by carrying out "exploratory" simulations using small system sizes for select combinations of Γ and λ values at large $\varepsilon_n = 2.5\varepsilon$ that promoted assembly. As detailed in Figure S9 and summarized in Figure 5B, nanocubes exhibit a propensity to self-assemble in mainly two regions of the parameter space: region \mathcal{R}_1 involving small Γ and small-to-moderate λ , and region \mathcal{R}_2 involving large Γ and moderate λ . Nanocubes at moderate to high grafting density Γ generally remain largely dispersed due to strong steric repulsion from the grafts. Nanocubes with grafts of high relative miscibility λ also cannot assemble because of the chain-stretching effect discussed earlier: these grafts that interact similarly with both polymer layers stretch out at the interface, generating strong steric repulsion between nanocubes (Figure S8A and B), which must either squeeze these stretched chains or displace them away from the interface to form close contacts. The unexpected assembly behavior observed in \mathcal{R}_2 likely arises from the inability of the matrix chains to "wet" the dense graft corona around the nanocubes. 44,45 Such "surface tension" between corona and matrix leads to attraction between nanocubes that is especially strong for those grafted with chains of moderate miscibility λ . The reason is that such nanocubes lie face-up at the interface (Figure 3C), so their graft-covered sides are parallel to each other and present a large area of contact. Nanocubes with grafts of lower or higher relative miscibility exhibit edge-up and vertex-up orientations that present much smaller areas of contact, leading to weaker attraction between nanocubes. The high-miscibility grafts also lead to steric repulsion due to chain stretching, which further inhibits assembly.

On the basis of these results, we focused on studying the assembly behavior of polymer-grafted nanocubes in regions \mathcal{R}_1 and \mathcal{R}_2 of the parameter space. By performing simulations with larger systems of particles, we were able to access the higherorder assemblies formed by these nanocubes. Figure 5C-E present the structures achieved through assembly of nanocubes with grafts of negligible miscibility at low grafting density (λ = 0-0.2 and $\Gamma = 0.16$ chains/ σ^2) belonging to \mathcal{R}_1 . At weak interparticle interaction strengths ($\varepsilon_{\rm n} = 0.5\varepsilon = 0.5k_{\rm B}T$), the nanocubes form a perforated square-ordered monolayer held together by edge-edge and tip-tip contacts between adjacent nanocube cores (Figure 5C). The individual nanocubes in the monolayer exhibit a vertex-up orientation with some disorder and remain largely submerged within p₁, unchanged from their configuration in isolation (see Figure 3A). Despite their sparse grafting, the grafts can still exert sufficient steric repulsion (due

to their extended conformations in p₁, which is a good solvent for the grafts) to prevent nanocubes from assembling into a more close-packed structure. The porous framework helps to accommodate the grafts without incurring much steric repulsion while still allowing for favorable contacts between adjacent nanocubes *via* their edges and tips.

At higher interaction strengths ($\varepsilon_n=1.2\varepsilon$), the nanocubes prefer to assemble into a perforated hexagonally ordered monolayer (Figure 5D), where nanocubes exhibit stricter vertex-up orientations and edge—edge contacts between adjacent particles. These contacts are stronger than tip—tip contacts, and they also impose stronger geometrical constraints on the relative orientations of the contacting nanocubes. Both these factors contribute toward the formation of the observed architecture, where stronger edge—edge contacts help overcome the stronger steric repulsion between the grafts within these pores, which are now donated by six nanocubes, rather than four as in the case of the square-ordered monolayers above.

The interparticle interactions are however still not strong enough to fully overcome the steric repulsion to form a close-packed structure. We therefore conjectured that we might be able to achieve such assemblies by either reinforcing the interparticle attraction between nanocube cores or reducing steric repulsion from grafts. Indeed, our simulations showed that increasing the value of $\varepsilon_{\rm n}$ to 2.5ε and slightly enhancing the relative miscibility of grafts to $\lambda=0.2$ (which helps to reduce the steric repulsion between the grafted nanocubes, as the grafts tend to stretch toward the interface and away from the contact points between the nanocube cores) led to the targeted close-packed monolayer structure (Figure 5E).

Nanocubes grafted with chains of more moderate relative miscibility ($\lambda = 0.6$) at similarly low grafting density and high interaction strength (Γ = 0.16 chains/ σ^2 and ε_n = 2 ε) at the rightmost edge of \mathcal{R}_1 also displayed a tendency to assemble, though interestingly these particles formed strings of vertex-up nanocubes held together by edge-edge contacts (Figure 5F). Due to the higher miscibility of their grafts with p2, these nanocubes are less asymmetrically positioned at the interface, leading to some protrusion of grafts into p₂. Due to the slightly poor solvent quality of p₂ for the grafts, these protruding portions of grafts introduce a weak attraction between the nanocubes. However, the portions of grafts remaining in p₁ (which is a good solvent for the grafts) extend outward and lead to steric repulsion between nanocubes. Together, these effects produce a net attraction between the nanocubes that promotes their assembly as well as multibody steric forces between the extended grafts that disfavor assembly into more closed structures such as the perforated and close-packed frameworks obtained above.

Within region \mathcal{R}_2 , nanocubes grafted with chains of moderate miscibility at very high grafting density ($\lambda=0.4$ and $\Gamma=1.0$ chains/ σ^2) formed a hexagonally close-packed monolayer (Figure 5G) in which the nanocube cores are well separated from each other by the dense corona of grafts surrounding each core. Clearly, such assembly configuration with face-up nanocubes that maximizes the number of contacts and the area of each contact between the graft corona on nanocubes minimizes the exposure of the grafts to the surrounding polymer, which is a bad solvent for them in this high-grafting regime, as discussed earlier.

We also examined the coassembly of *two* species of polymer-grafted nanocubes trapped in different planes parallel to the

ı

interface. For convenience, we considered "antisymmetric" species, where the particles are identical in all aspects except that they are grafted with chains compatible with opposite polymer layers. In isolation, the two species of particles would prefer to reside asymmetrically on opposite sides of the interfacial plane while still intersecting with it. While such antisymmetric particles were found to assemble into a range of bilayer superlattices in the case of polymer-grafted spherical NPs (ref 27 and unpublished data), we found it considerably more challenging to achieve uniform assemblies with antisymmetric polymer-grafted nanocubes (Figure S10). The reason is that for assembly to occur the two species of nanocubes need to orient in a manner that permits not only strong contacts between particles of the same species in the direction parallel to the interface (which we showed to occur only in the narrow regions \mathcal{R}_1 and \mathcal{R}_2) but also strong contacts across particle species in the direction normal to the interface.

One ordered structure we were able to achieve from coassembly of two antisymmetric species of nanocubes is the 1D ribbon shown in Figure 5H. This structure was assembled from \mathcal{R}_1 -nanocubes of moderate interaction strength $(\varepsilon_n = \varepsilon)$ grafted sparsely with chains completely immiscible with p_2 (Γ = 0.16 chains/ σ^2 and λ = 0). The nanocubes exhibit a roughly vertex-up orientation in the structure and mediate "lateral" contacts with two nanocubes in the same layer via diagonally opposite edges and "vertical" contact with one nanocube in the opposite layer via a third edge. To maximize these interactions, the nanocube cores exhibit some face-to-face overlap in each edge-mediated contact, leading to the "stepped" topography seen in Figure 5H. Due to the tilted orientation of nanocubes and the large energy penalty for deviating from their equilibrium position near the interfacial plane, the nanocubes from opposite layers bind to each other at tilted angles with respect to the normal of the interfacial plane. As a result of these constraints, the nanocubes can form contacts in only one lateral direction, and assembly is prevented in the other lateral direction due to steric clashes between the nanocube cores, explaining the 1D nature of the assembled structure. While antisymmetric species of nanocubes from region \mathcal{R}_2 also displayed some tendency to assemble across the interfacial plane to yield interdigitated bilayers, the assembled structures were finite-sized and exhibited significant disorder (Figure

Lastly, we examined the degree and periodicity of ordering of nanocubes in the structural phases obtained here by computing their radial distribution function (RDF) and 2D bond orientational order parameters 46,47 (Figure S12). The RDFs show that all phases are strongly ordered, displaying sharp peaks at their expected "crystallographic" locations. Of note, the RDFs can distinguish between the two string phases (Figure S12A and E) and the four monolayer phases (Figure S12B-D and F). The order parameters further indicate that the square-ordered monolayer possesses strong 4-fold symmetry, and the perforated hexagonally ordered monolayer and the hexagonally close-packed monolayer show a high degree of 6-fold symmetry (Figure S12H). Given that the perforated structures (Figure 5C-E) enclose a significant number of polymer grafts in their voids, we also investigated the structural order of these grafts by computing their segment-based RDFs. Our results suggest that these grafts are present in a disordered, liquid-like state (Figure S13).

CONCLUSIONS

We present a strategy to control the orientation of faceted NPs, constrain their motion to two dimensions, and harness the resulting anisotropic interactions between the particles to assemble them into unique low-dimensional structures. The approach involves using a fluid-fluid interface to trap NPs at or near the interfacial plane, which enforces planarity in interparticle interactions, and surface-grafting of NPs with functional groups, whose differences in miscibility with the interface-forming fluids determines the orientation and normal position of the faceted NPs relative to the interfacial plane. To demonstrate feasibility of this approach, we used computer simulations to predict the orientational and assembly behavior of polymer-grafted nanocubes at the interface between two mutually immiscible polymer melts. While bare nanocubes that interacted similarly with both polymer layers adopted a vertexup orientation at the interface, the orientation of polymergrafted nanocubes could be tuned between face-up, edge-up, and vertex-up orientations based on the surface density and relative miscibility of the grafts with the two layers. We further showed how NP orientation is governed by an interplay between the interfacial area occluded by the nanocube, the difference in the miscibility of the grafts with the two polymer layers, and the degree of stretching and intercalation of grafts at the interface. By taking advantage of these different graftinduced orientations of nanocubes, we demonstrated their assembly into unique structures such as rectilinear strings, close-packed sheets, ribbons, and perforated sheets, architectures challenging to obtain through bulk assembly of faceted NPs or interfacial assembly of spherical NPs. Several of these predicted structures have been reproduced in experiments; for instance, Ling et al. obtained strings and hexagonally packed monolayers of Ag nanocubes at an oil/water interface where a binary mixture of hydrophilic and hydrophobic grafts was used to control the interfacial displacement of nanocubes. 32,48 Further experimental work would be needed to validate the assembly of the other structures presented here, especially the perforated sheet and ribbon phases (Figure 5).

Faceted NPs of noble metals support complex surface plasmon resonance modes when organized into close but noncontacting structures. 15,32 These modes are sensitive to not only the gap size between NPs but also their relative orientation and higher-order arrangement. Our interfacial assembly approach, which yields unique arrangements of particles with nanoscopic gaps and tunable orientations due to steric repulsion from polymer grafts, could therefore be ideal for fabricating new plasmonic materials. Among the assemblies obtained here, the nanocube strings would be expected to produce a linear array of highly intense, localized electromagnetic "hotspots" potentially useful for sensing if the nanocubes were made of noble metals.³² The hexagonally close-packed sheets of nanocubes, in comparison, should yield less intense but larger areas of field concentration recently shown to yield strong enhancement in Raman spectra.³² The percolated nanocube sheets could be attractive candidates as optical absorbers for solar energy harvesting.⁴⁹ The ability of our approach to arrange surfaces from different species of nanocubes close to each other, as in the case of the bilayer ribbons discussed earlier, could be exploited for carrying out multistage chemical reactions that require multiple catalytic surfaces in proximity. Lastly, the approach can yield percolated monolayers of particles that could find applications

as membranes.⁵⁰ Thus, interfacial assembly of faceted NPs provides a viable avenue for fabricating low-dimensional materials with diverse potential applications.

This study also advances the importance of interfacial deformations on the orientation of faceted NPs and shows how ignoring such deformations could lead to erroneous predictions of orientation.^{33,42} Indeed, naïve calculations of the interfacial area occluded by nanocubes assuming a perfectly thin and flat interface wrongly predict the edge-up orientation as the most favored orientation, while our calculations accounting for the true deformation of the interface correctly predicted the vertex-up orientation as the favored orientation. Also advanced in this work is our automated procedure for classifying arbitrary orientations of nanocubes at surfaces based on projected areas of their facets, an approach that could find applications in other fields such as geometry, image analysis, and microscopy.

While this work focused on the behavior of polymer-grafted nanocubes at planar interfaces, the studies can be readily extended to cylindrical and spherical fluid-fluid interfaces, such as those observed in oil—water emulsions, ⁵¹ and to other anisotropic particle shapes. ^{15–17} Furthermore, the effects of parameters such as particle size, its surface affinity, curvature of its edges, and free and grafted polymer chain lengths currently held fixed could be investigated in future studies. In particular, the surface affinity of the nanocube core, currently assumed to be neutral to both layers making up the interface, could perturb the interfacial displacement of polymer-grafted nanocubes, particularly at low grafting densities. Particle size could impact the relative strength of interparticle interactions in the edgeedge, face-face, and vertex-vertex contact configurations, 34 and thereby their assembly configuration. The curvature of shaped particles can play a role in the adsorption and distribution of polymer chains on the surface 52-54 and impact the interfacial area occluded by the particle. The relative lengths of the free and grafted chains are known to affect their wetting properties.44 The role of interfacial deformation on particle orientation and assembly could also be examined in more depth and applied to these other particle-interface systems. Lastly, it would also be useful to develop a comprehensive theoretical model in the future to predict the interfacial orientation of polymer-grafted shaped NPs that accounts for not only the effects of polymer graft conformation in the two layers on the interfacial occluded area but also the effect of particle shape on interfacial deformation and stretching of chains at the interface.

METHODS

Coarse-Grained Model. To investigate the dynamics of polymer-grafted nanocubes in the polymer bilayer, we extended the model we previously used for studying the assembly of polymer-grafted spherical NPs at polymer interfaces. All polymer chains in the system were treated as Kremer–Grest bead-chains, 37 where short segments of the chain are described by beads of size σ and mass m. We used chain lengths of $L_{\rm g}=5$ and $L_{\rm p}=10$ beads to describe the grafts and the two polymers making up the bilayer, respectively (Figure 1A).

Adjacent beads in the chains, denoting bonded segments, interacted with each other through finitely extensible nonlinear elastic (FENE) spring and Weeks—Chandler—Anderson (WCA) potentials. ⁵⁵ The FENE spring potential, which ensures that bonded segments do not stretch beyond a cutoff distance, is given by

$$U_{\text{FENE}}(r; k, R_0) = -\frac{k}{2} R_0^2 \ln \left[1 - \left(\frac{r}{R_0} \right)^2 \right]$$
 (1)

where r is the separation distance between the segments, $k=30\varepsilon/\sigma^2$ is the spring constant, ε is the characteristic energy parameter, and $R_0=1.5\sigma$ is the maximum possible length of the spring. The WCA potential, a short-range purely repulsive potential that models excluded-volume interactions between the bonded segments, can be conveniently presented in the form of a cut-and-shifted Lennard-Jones (LJ) potential:

$$U_{LJ}(r; \sigma, \varepsilon, r_{c}) = \begin{cases} 4\varepsilon \left[\left(\frac{\sigma}{r}\right)^{12} - \left(\frac{\sigma}{r}\right)^{6} - \left(\frac{\sigma}{r_{c}}\right)^{12} + \left(\frac{\sigma}{r_{c}}\right)^{6} \right] & r < r_{c} \\ 0 & r \ge r_{c} \end{cases}$$
(2)

with a cutoff distance of $r_c = 2^{1/6}\sigma$.

Interactions between nonbonded segments were treated based on the miscibility of their parent chains. Chains of the same polymer type were considered fully miscible; thus, pairs of segments within a chain or across chains of the same type interacted with each other via the LJ potential $U_{LI}(r; \sigma, \varepsilon, r_c = 2.5\sigma)$, which accounts for both attractive and the excluded-volume interactions due to the larger cutoff of $r_c = 2.5\sigma$. The two polymer layers were considered mutually immiscible, so their segments interacted with each other via the WCA potential $U_{\rm LI}(r; \sigma_r)$ ε , $r_c = 2^{1/6} \sigma$), which accounts for excluded-volume interactions only. The grafts were assumed to be fully miscible with one polymer layer, so their intersegment interactions were also treated by the LJ potential $U_{\rm LJ}(r; \sigma, \varepsilon, r_{\rm c}=2.5\sigma)$. Depending on the system being studied, the grafts were either immiscible, partially miscible, or fully miscible with the other polymer layer: when immiscible, the graft segments interacted with this layer via the WCA potential $U_{\rm LJ}(r; \sigma, \varepsilon, r_{\rm c} =$ $2^{1/6}\sigma$); when partially miscible, the segments interacted via the LJ potential $U_{\rm LI}(r; \sigma, \lambda \varepsilon, r_{\rm c} = 2.5\sigma)$ with a reduced attraction strength of $\lambda \varepsilon$, where $0 < \lambda < 1$, and when fully miscible, they interacted *via* the original LJ potential $U_{\rm LJ}(r; \sigma, \varepsilon, r_{\rm c} = 2.5\sigma)$.

The nanocubes were modeled as rigid bodies constructed out of a simple-cubic 5 \times 5 \times 5 lattice of coarse-grained beads, each of size σ for convenience (Figure 1A). The grafts were attached to the surface beads of the nanocubes via the combined FENE-WCA potential. We explored grafting densities of $\Gamma = 0.16-1.0$ chains/ σ^2 , resulting in chain conformations spanning the mushroom to brush regimes. The excluded volume interactions between the nanocubes and surrounding polymer chains were also treated using a WCA potential $U_{\rm LJ}(r; \sigma,$ ε , $r_c = 2^{1/6} \sigma$) acting between individual nanocube and polymer beads. The vdW interaction between nanocubes was calculated as the summation of the LJ potential $U_{\rm LJ}(r; \sigma, \varepsilon_{\rm n}, r_{\rm c} = 2.5\sigma)$ across all pairs of beads constituting the interacting nanocubes. In this work, the nanocube-nanocube interbead attraction strength was set to $\varepsilon_{\rm n}$ = $0.5-2.5\varepsilon$, which resulted in a net attraction of roughly $-75\varepsilon_{\rm n}$ between bare nanocubes in perfect face-face contact. Overall, this simplified model contains three adjustable parameters $(\lambda, \Gamma, \text{ and } \varepsilon_n)$ expected to govern the interfacial orientation and assembly of polymer-grafted nanocubes, with parameters σ and ε specifying the length and energy scales of the system.

Molecular Dynamics Simulations. We used the LAMMPS package ⁵⁶ to carry out MD simulations of the nanocube–polymer system. All simulations were carried out in the canonical (NVT) ensemble at a temperature of $\varepsilon/k_{\rm B}$ and a polymer density of 0.85 beads/ σ^3 , so that the bilayer is present in a melt-like state. A velocity-Verlet algorithm with a time step of $0.002(m\sigma^2/\varepsilon)^{1/2}$ (where m is the mass of a polymer bead) and a Nosé–Hoover thermostat with a time constant of $1.0(m\sigma^2/\varepsilon)^{1/2}$ were used for integrating the equations of motion and controlling the system temperature. Two impermeable LJ walls were used to confine the polymer bilayer in the z direction normal to the interface, while periodic boundary conditions were applied to the x and y directions parallel to the interface. To capture the entire range of influence of the interface and avoid distortion from

the enclosing walls, each polymer layer was chosen to have a sufficiently large thickness of 20σ , given that the polymer-grafted nanocubes are roughly of effective diameter 5σ to 11σ depending on the grafting density. The simulation box was also kept sufficiently large in the two lateral directions to ensure that NPs or their aggregates do not indirectly interact with their images through hydrodynamic flows propagated through the periodic boundaries in the lateral direction. A padding of 15σ in each lateral direction about the NP structures was found to be sufficient for this purpose.

To generate a well-equilibrated system of bare or polymer-grafted nanocubes dispersed in the polymer bilayer, we placed the required numbers of nanocubes and matrix polymer chains of the two layers in a simulation box ~50 times larger than the final desired dimensions to prevent steric overlaps in the initial configuration. The nanocube centers were placed sufficiently far from each other along the z = 0plane with nanocube faces parallel/perpendicular to the z direction. The polymer grafts on the nanocubes were arranged in straight conformations normal to their surfaces. The chains of layers p₁ and p₂ were organized as loose bundles of straight chains and placed above (z> 0) and below (z < 0) the nanocubes. Maxwell-Boltzmann distributed velocities were assigned to all polymer segments, and MD simulations were performed for 0.1-0.4 million time steps while holding the nanocubes fixed at their initial positions and orientations. The simulation box was then slowly compressed over 1 million time steps until it reached the required dimensions and the two matrix polymers had phase-separated into a stable bilayer. Meanwhile, the nanocubes were rotated about their own axes and translated to the desired orientation and position in the simulation box (see below). While keeping the nanocubes fixed, we continued the MD simulations for an additional 1 million time steps to further equilibrate the system.

Following equilibration, we carried out two different sets of simulations. The first set is equilibrium simulations of *freely mobile* nanocubes within the bilayer used for exploring the orientational behavior and self-assembly of nanocubes. In these simulations, the nanocubes were released from the fixed positions and orientations at the interfacial plane they held during the equilibration step. We found that the final orientation, *z*-position, and, in many cases, the assembled structure these nanocubes adopted were insensitive to their initial orientation and position. These simulations were typically performed for 12 million time steps, and the trajectories of the NPs were recorded every 100 time steps.

The second set involves simulations for computing the potential of mean force (PMF) of a single nanocube constrained in its three principal orientations as a function of their normal coordinate z. These simulations were started from configurations generated during the equilibration step in which the nanocubes were rotated to (0°, 0°), $(45^{\circ}, 0^{\circ})$, or $(54.7^{\circ}, 45^{\circ})$ for them to exhibit pure face-up, edgeup, or vertex-up orientation, respectively. Keeping the orientation of the nanocube fixed, the center of the nanocube was successively held fixed at equidistant points (spaced $\Delta z = 0.5\sigma$ apart) along a normal path starting in the bulk region of one polymer layer at $z_0 = -8\sigma$ (or $z_0 = -10\sigma$ for a nanocube with higher grafting densities) until it reached the interfacial plane at z = 0. Specifically, the nanocube center was held fixed for 0.6 million time steps at each z location, and the ensemble averaged normal force $\langle f_z(t) \rangle$ experienced by the entire nanocube (including grafts) was measured from the last 0.5 million time steps. At their initial positions z_0 , nanocubes were fully immersed in the bulk of the bottom layer, where the net force $f_z(z_0)$ experienced by the nanocube is expected to be zero. Therefore, the PMF corresponding to each orientation can be computed by simply integrating their corresponding force components over positions as

$$\Delta F(z) = -\int_{z_0}^{z} f_z(z) \, \mathrm{d}z \tag{3}$$

Furthermore, because all three orientations have the same free energy at this bulk-like position z_0 , all three PMFs are relative to the same reference free energy, so differences in PMF values at a common z value across the three orientations represents true differences in free energies across the orientations. More details are provided in our earlier publication. 26

Details of Orientation Classification. Our method for classifying nanocube orientations relies on computing the surface-projected areas of its three faces with respect to the interfacial plane. Those areas (normalized by face area) can be calculated by $S_i = |\mathbf{n} \cdot \mathbf{c}_i|$, where i = 1, 2, and 3, \mathbf{n} is a unit vector normal to the interfacial place, and \mathbf{c}_i are three unit vectors describing the internal axes of the nanocube. Since these axes are orthogonal to each other, the projected areas can be expressed in terms of the polar angle θ and the internal Euler angle Φ by $S_1 = \cos \theta$, $S_2 = \sin \theta \cos \Phi$, and $S_3 = \sin \theta \sin \Phi$.

Based on our earlier discussion, (θ, Φ) can be defined so that $S_1 \ge S_2 \ge S_3$ (see also Figure S1). To determine θ and Φ of an arbitrarily oriented nanocube, we outputted the coordinates of the beads making the cube from which vectors $\mathbf{c}_i = (c_{ix}, c_{iy}, c_{iz})$ were obtained. θ was then defined as the smallest angle between \mathbf{n} and \mathbf{c}_i , which can be obtained via $\theta = \operatorname{arc\ cosln} \cdot \mathbf{c}_p |$ (where p is the index i that yields the maximum $|c_{iz}|$). To determine Φ , a new unit vector that is orthogonal to both \mathbf{n} and \mathbf{c}_p was constructed: $\mathbf{e} = (\mathbf{n} \times \mathbf{c}_p)/|\mathbf{n} \times \mathbf{c}_p|$. Φ was then obtained as the smaller of the two angles formed between \mathbf{e} and the remaining two \mathbf{c}_i ($i \neq p$), calculated as arc $\operatorname{cosle} \cdot \mathbf{c}_i$ l. The (θ, Φ) obtained in this manner could then be classified into one of the three principal orientations based on the projected-area partition criterion discussed earlier.

Specifically, the internal boundary l_{fe} between face-up and edge-up orientations (Figure 1E) is determined by the condition that the fraction of projected area contributed by the dominant face is 3/4 (midpoint of fractions 1/2 and 1 contributed by the dominant face in "pure" edge- and face-up orientations); that is, $S_1/(S_1 + S_2 + S_3) = 3/(S_1 + S_2 + S_3) = 3/(S_1 + S_2 + S_3)$ 4. This condition can be mapped onto (θ, Φ) as $\cos \theta/(\cos \theta + \sin \theta)$ $\cos \Phi + \sin \theta \sin \Phi$) = 3/4, resulting in the following equation for $l_{\rm fe}$: $\tan \theta = 1/(3 \sin \Phi + 3 \cos \Phi)$ (or $\theta = \tan^{-1}[1/(3 \sin \Phi + 3 \cos \Phi)]$). Similarly, the internal boundary l_{ev} between edge-up and vertex-up orientations is determined by the condition that the fraction of the projected area contributed by the top-two dominant faces is 5/6 (midpoint of the fractions in pure vertex- and edge-up orientations), or $(S_1 + S_2)/(S_1 + S_2 + S_3) = 5/6$, which can be mapped back to (θ, θ) Φ) as $(\cos \theta + \sin \theta \cos \Phi)/(\cos \theta + \sin \theta \cos \Phi + \sin \theta \sin \Phi) = 5/$ 6, resulting in the following equation for $l_{\rm ev}$: tan θ = 1/(5 sin Φ – $\cos\Phi$) (or $\theta = \tan^{-1}[1/(5 \sin \Phi - \cos \Phi)]$). The two internal boundaries combined with the four outer boundaries (see Figure S1) define the angle bounds for three principal orientations of nanocubes on surfaces.

Determining the Interface Shape. To calculate the effective area of the interface from our MD simulations, we would need to first determine the instantaneous position of the undulating interface. To this end, the simulation box was divided into $M \times N$ cells in the xy plane (in our study M = N = 30). We then searched along the vertical direction within each cell to locate the closest pair of beads (in the z direction) from opposite polymer layers. The midplane between two xy planes passing through the two identified beads was considered as the position of the interface within that grid. The instantaneous undulating interface was then obtained by connecting the center points of the midplanes in each cell (see Figure 2D). The overall surface area of the instantaneous interface was retrieved by summing up the areas of the triangle elements made by those center points. The interfacial area was computed every 10 time steps, and averaging these areas over 0.5 million time steps gave the effective interfacial area.

Bond Orientational Order Parameter Calculations. The 2D bond orientational order parameters for k-fold symmetry were computed by 46,47

$$\phi_{k,n}^{a} = \frac{1}{n} \sum_{b \in \text{NN}(a)}^{n} e^{ik\theta_{ab}}$$
(4)

where NN(a) is the set of nearest neighbors of nanocube a, n is the number of nearest neighbors, and θ_{ab} is the angle between the nanocube-pair vector \mathbf{r}_{ab} drawn from the center of nanocube a to nanocube b and the positive x-axis. The averaged scalar parameter $\phi_k = \langle |\phi_{kn}|^a | \rangle$ was then reported.

ASSOCIATED CONTENT

Supporting Information

The Supporting Information is available free of charge at https://pubs.acs.org/doi/10.1021/acsnano.1c10416.

Degeneracy of orientation space; interfacial displacements, orientational angles, and assembly outcomes of bare nanocubes and polymer-grafted nanocubes as a function of grafting density and graft relative miscibility; contour maps of polymer segment density; cross-sectional area of bare cubes; occluded interfacial area of polymer-grafted nanocubes; interaction free energy between bare and between polymer-grafted nanocubes; assembly outcomes of antisymmetric polymer-grafted nanocubes with dense grafts and with low relative-miscibility grafts; and structural analyses of assembled nanocubes and their grafts at the interface (PDF)

AUTHOR INFORMATION

Corresponding Author

Gaurav Arya — Department of Mechanical Engineering and Materials Science, Duke University, Durham, North Carolina 27708, United States; orcid.org/0000-0002-5615-0521; Phone: +1 (919) 660-5435; Email: gaurav.arya@duke.edu; Fax: +1 (919) 660-8963

Authors

Yilong Zhou — Department of Mechanical Engineering and Materials Science, Duke University, Durham, North Carolina 27708, United States; orcid.org/0000-0002-5610-826X

Tsung-Yeh Tang — Department of NanoEngineering, University of California, San Diego, La Jolla, California 92093, United States

Brian Hyun-jong Lee – Department of Mechanical Engineering and Materials Science, Duke University, Durham, North Carolina 27708, United States

Complete contact information is available at: https://pubs.acs.org/10.1021/acsnano.1c10416

Notes

The authors declare no competing financial interest.

ACKNOWLEDGMENTS

This work was sponsored by the National Science Foundation (Grant No. CMMI 1636356) and by the UC San Diego Materials Research Science and Engineering Center (UCSD MRSEC) supported by the National Science Foundation (Grant No. DMR-2011924). Computational resources were provided by the Duke Computing Cluster (DCC) and the Extreme Science and Engineering Discovery Environment (XSEDE) Program supported by the National Science Foundation (Grant No. ACI-1053575).

REFERENCES

- (1) Sacanna, S.; Korpics, M.; Rodriguez, K.; Colón-Meléndez, L.; Kim, S. H.; Pine, D. J.; Yi, G. R. Shaping Colloids for Self-Assembly. *Nat. Commun.* **2013**, *4*, 2–7.
- (2) Damasceno, P. F.; Engel, M.; Glotzer, S. C. Predictive Self-Assembly of Polyhedra into Complex Structures. *Science* **2012**, 337 (6093), 453–457.
- (3) Sacanna, S.; Irvine, W. T. M.; Chaikin, P. M.; Pine, D. J. Lock and Key Colloids. *Nature* **2010**, *464* (7288), 575–578.

- (4) Glotzer, S. C.; Solomon, M. J. Anisotropy of Building Blocks and Their Assembly into Complex Structures. *Nat. Mater.* **2007**, *6* (8), 557–562.
- (5) Sherry, L. J.; Chang, S. H.; Schatz, G. C.; Van Duyne, R. P.; Wiley, B. J.; Xia, Y. Localized Surface Plasmon Resonance Spectroscopy of Single Silver Nanocubes. *Nano Lett.* **2005**, *5* (10), 2034–2038.
- (6) Rui Tan, J. M.; Ruan, J. J.; Lee, H. K.; Phang, I. Y.; Ling, X. Y. A Large-Scale Superhydrophobic Surface-Enhanced Raman Scattering (SERS) Platform Fabricated via Capillary Force Lithography and Assembly of Ag Nanocubes for Ultratrace Molecular Sensing. *Phys. Chem. Chem. Phys.* **2014**, *16* (48), 26983–26990.
- (7) Deori, K.; Gupta, D.; Saha, B.; Deka, S. Design of 3-Dimensionally Self-Assembled CeO2 Nanocube as a Breakthrough Catalyst for Efficient Alkylarene Oxidation in Water. *ACS Catal.* **2014**, 4 (9), 3169–3179.
- (8) Zhang, S.; Fan, W.; Panoiu, N. C.; Malloy, K. J.; Osgood, R. M.; Brueck, S. R. J. Experimental Demonstration of Near-Infrared Negative-Index Metamaterials. *Phys. Rev. Lett.* **2005**, *95* (13), 1–4.
- (9) Hentschel, M.; Saliba, M.; Vogelgesang, R.; Giessen, H.; Alivisatos, A. P.; Liu, N. Transition from Isolated to Collective Modes in Plasmonic Oligomers. *Nano Lett.* **2010**, *10* (7), 2721–2726.
- (10) Shin, D.; Urzhumov, Y.; Lim, D.; Kim, K.; Smith, D. R. A Versatile Smart Transformation Optics Device with Auxetic Elasto-Electromagnetic Metamaterials. Sci. Rep. 2015, 4, 1–9.
- (11) Pietrobon, B.; McEachran, M.; Kitaev, V. Synthesis of Size-Controlled Faceted Pentagonal Silver Nanorods with Tunable Plasmonic Properties and Self-Assembly of These Nanorods. ACS Nano 2009, 3 (1), 21–26.
- (12) Müller, C. M.; Mornaghini, F. C. F.; Spolenak, R. Ordered Arrays of Faceted Gold Nanoparticles Obtained by Dewetting and Nanosphere Lithography. *Nanotechnology* **2008**, *19* (48), 485306.
- (13) Peng, X.; Manna, L.; Yang, W.; Wickham, J. Shape Control of CdSe Nanocrystals. *Nature* **2000**, *404*, 59–61,.
- (14) Tao, A. R.; Habas, S.; Yang, P. Shape Control of Colloidal Metal Nanocrystals. *Small* **2008**, *4* (3), 310–325.
- (15) Gao, B.; Arya, G.; Tao, A. R. Self-Orienting Nanocubes for the Assembly of Plasmonic Nanojunctions. *Nat. Nanotechnol.* **2012**, *7* (7), 433–437.
- (16) Gurunatha, K. L.; Marvi, S.; Arya, G.; Tao, A. R. Computationally Guided Assembly of Oriented Nanocubes by Modulating Grafted Polymer-Surface Interactions. *Nano Lett.* **2015**, *15* (11), 7377–7382.
- (17) Hsiao, L. C.; Schultz, B. A.; Glaser, J.; Engel, M.; Szakasits, M. E.; Glotzer, S. C.; Solomon, M. J. Metastable Orientational Order of Colloidal Discoids. *Nat. Commun.* **2015**, *6* (1), 1–8.
- (18) Genix, A. C.; Oberdisse, J. Nanoparticle Self-Assembly: From Interactions in Suspension to Polymer Nanocomposites. *Soft Matter* **2018**, *14* (25), 5161–5179.
- (19) Akcora, P.; Liu, H.; Kumar, S. K.; Moll, J.; Li, Y.; Benicewicz, B. C.; Schadler, L. S.; Acehan, D.; Panagiotopoulos, A. Z.; Pryamitsyn, V. Anisotropic Self-Assembly of Spherical Polymer-Grafted Nanoparticles. *Nat. Mater.* **2009**, *8* (4), 354–359.
- (20) Kim, B. J.; Fredrickson, G. H.; Hawker, C. J.; Kramer, E. J. Nanoparticle Surfactants as a Route to Bicontinuous Block Copolymer Morphologies. *Langmuir* **2007**, 23 (14), 7804–7809.
- (21) Gerdon, A. E.; Oh, S. S.; Hsieh, K.; Ke, Y.; Yan, H.; Soh, H. T. Controlled Delivery of DNA Origami on Patterned Surfaces. *Small* **2009**, *5* (17), 1942–1946.
- (22) Rycenga, M.; Camargo, P. H. C.; Xia, Y. Template-Assisted Self-Assembly: A Versatile Approach to Complex Micro-and Nanostructures. *Soft Matter* **2009**, *5* (6), 1129–1136.
- (23) Wang, Y.; Wang, Y.; Breed, D. R.; Manoharan, V. N.; Feng, L.; Hollingsworth, A. D.; Weck, M.; Pine, D. J. Colloids with Valence and Specific Directional Bonding. *Nature* **2012**, *491* (7422), 51–55.
- (24) Erb, R. M.; Son, H. S.; Samanta, B.; Rotello, V. M.; Yellen, B. B. Magnetic Assembly of Colloidal Superstructures with Multipole Symmetry. *Nature* **2009**, *457* (7232), 999–1002.

- (25) Cai, Y.; Zhang Newby, B. Marangoni Flow-Induced Self-Assembly of Hexagonal and Stripelike Nanoparticle Patterns. *J. Am. Chem. Soc.* **2008**, *130* (19), 6076–6077.
- (26) Tang, T. Y.; Arya, G. Anisotropic Three-Particle Interactions between Spherical Polymer-Grafted Nanoparticles in a Polymer Matrix. *Macromolecules* **2017**, *50* (3), 1167–1183.
- (27) Tang, T. Y.; Zhou, Y.; Arya, G. Interfacial Assembly of Tunable Anisotropic Nanoparticle Architectures. *ACS Nano* **2019**, *13* (4), 4111–4123.
- (28) Retsch, M.; Zhou, Z.; Rivera, S.; Kappl, M.; Zhao, X. S.; Jonas, U.; Li, Q. Fabrication of Large-area, Transferable Colloidal Monolayers Utilizing Self-assembly at the Air/Water Interface. *Macromol. Chem. Phys.* **2009**, 210 (3–4), 230–241.
- (29) Böker, A.; He, J.; Emrick, T.; Russell, T. P. Self-Assembly of Nanoparticles at Interfaces. *Soft Matter* **2007**, 3 (10), 1231–1248.
- (30) Shi, S.; Russell, T. P. Nanoparticle Assembly at Liquid–Liquid Interfaces: From the Nanoscale to Mesoscale. *Adv. Mater.* **2018**, *30* (44), 1–22.
- (31) Lin, Y.; Skaff, H.; Emrick, T.; Dinsmore, A. D.; Russell, T. P. Nanoparticle Assembly and Transport at Liquid-Liquid Interfaces. *Science* **2003**, 299 (5604), 226–229.
- (32) Yang, Y.; Lee, Y. H.; Phang, I. Y.; Jiang, R.; Sim, H. Y. F.; Wang, J.; Ling, X. Y. A Chemical Approach to Break the Planar Configuration of Ag Nanocubes into Tunable Two-Dimensional Metasurfaces. *Nano Lett.* **2016**, *16* (6), 3872–3878.
- (33) Shi, W.; Zhang, Z.; Li, S. Quantitative Prediction of Position and Orientation for Platonic Nanoparticles at Liquid/Liquid Interfaces. *J. Phys. Chem. Lett.* **2018**, 9 (2), 373–382.
- (34) Lee, B. H. J.; Arya, G. Orientational Phase Behavior of Polymer-Grafted Nanocubes. *Nanoscale* **2019**, *11* (34), 15939–15957.
- (35) Kronast, F.; Friedenberger, N.; Ollefs, K.; Gliga, S.; Tatibismaths, L.; Thies, R.; Ney, A.; Weber, R.; Hassel, C.; Florian, M. R.; Trunova, A. V.; Wirtz, C.; Hertel, R.; Hermann, A. D.; Farle, M. Element-Specific Magnetic Hysteresis of Individual 18 Nm Fe Nanocubes. *Nano Lett.* **2011**, *11* (4), 1710–1715.
- (36) Hao, J.; Wang, J.; Liu, X.; Padilla, W. J.; Zhou, L.; Qiu, M. High Performance Optical Absorber Based on a Plasmonic Metamaterial. *Appl. Phys. Lett.* **2010**, *96* (25), 10–13.
- (37) Kremer, K.; Grest, G. S. Dynamics of Entangled Linear Polymer Melts: A Molecular-Dynamics Simulation. *J. Chem. Phys.* **1990**, 92 (8), 5057–5086.
- (38) Hattemer, G. D.; Arya, G. Viscoelastic Properties of Polymer-Grafted Nanoparticle Composites from Molecular Dynamics Simulations. *Macromolecules* **2015**, 48 (4), 1240–1255.
- (39) Cheung, D. L. Molecular Dynamics Study of Nanoparticle Stability at Liquid Interfaces: Effect of Nanoparticle-Solvent Interaction and Capillary Waves. *J. Chem. Phys.* **2011**, *135* (5), 54704.
- (40) Galliero, G. Lennard-Jones Fluid-Fluid Interfaces under Shear. *Phys. Rev. E* **2010**, *81* (5), 56306.
- (41) Rezvantalab, H.; Shojaei-Zadeh, S. Tilting and Tumbling of Janus Nanoparticles at Sheared Interfaces. ACS Nano 2016, 10 (5), 5354–5361.
- (42) Soligno, G.; Dijkstra, M.; Van Roij, R. Self-Assembly of Cubes into 2D Hexagonal and Honeycomb Lattices by Hexapolar Capillary Interactions. *Phys. Rev. Lett.* **2016**, *116* (25), 1–6.
- (43) Gupta, U.; Hanrath, T.; Escobedo, F. A. Modeling the Orientational and Positional Behavior of Polyhedral Nanoparticles at Fluid-Fluid Interfaces. *Phys. Rev. Mater.* **2017**, *1* (5), 1–10.
- (44) Green, P. F. The Structure of Chain End-Grafted Nanoparticle/ Homopolymer Nanocomposites. *Soft Matter* **2011**, 7 (18), 7914–7926.
- (45) Frischknecht, A. L. Forces between Nanorods with End-Adsorbed Chains in a Homopolymer Melt. *J. Chem. Phys.* **2008**, *128* (22), 224902.
- (46) Anderson, J. A.; Antonaglia, J.; Millan, J. A.; Engel, M.; Glotzer, S. C. Shape and Symmetry Determine Two-Dimensional Melting Transitions of Hard Regular Polygons. *Phys. Rev. X* **2017**, *7* (2), 1–14.

- (47) Gupta, U.; Escobedo, F. A. Ligand Interactions and Nanoparticle Shapes Guide the Pathways toward Interfacial Self-Assembly. *Langmuir* **2022**, *38* (5), 1738–1747.
- (48) Yang, Y.; Lee, Y. H.; Lay, C. L.; Ling, X. Y. Tuning Molecular-Level Polymer Conformations Enables Dynamic Control over Both the Interfacial Behaviors of Ag Nanocubes and Their Assembled Metacrystals. *Chem. Mater.* **2017**, *29* (14), 6137–6144.
- (49) Rashidi, S.; Esfahani, J. A.; Rashidi, A. A Review on the Applications of Porous Materials in Solar Energy Systems. *Renew. Sustain. Energy Rev.* **2017**, 73, 1198–1210.
- (50) Berry, V.; Rangaswamy, S.; Saraf, R. F. Highly Selective, Electrically Conductive Monolayer of Nanoparticles on Live Bacteria. *Nano Lett.* **2004**, *4* (5), 939–942.
- (51) Gavrielatos, I.; Mohan, R.; Shoham, O. Effect of Intermediate Wettability Nanoparticles on Oil-Water Emulsion Stability. *J. Pet. Sci. Eng.* **2017**, *152*, *664*–*674*.
- (52) Choueiri, R. M.; Galati, E.; Thérien-Aubin, H.; Klinkova, A.; Larin, E. M.; Querejeta-Fernández, A.; Han, L.; Xin, H. L.; Gang, O.; Zhulina, E. B. Surface Patterning of Nanoparticles with Polymer Patches. *Nature* **2016**, *538* (7623), 79–83.
- (53) Villarreal, E.; Li, G. G.; Zhang, Q.; Fu, X.; Wang, H. Nanoscale Surface Curvature Effects on Ligand—Nanoparticle Interactions: A Plasmon-Enhanced Spectroscopic Study of Thiolated Ligand Adsorption, Desorption, and Exchange on Gold Nanoparticles. *Nano Lett.* **2017**, *17* (7), 4443—4452.
- (54) Lu, F.; Vo, T.; Zhang, Y.; Frenkel, A.; Yager, K. G.; Kumar, S.; Gang, O. Unusual Packing of Soft-Shelled Nanocubes. *Sci. Adv.* **2019**, 5 (5), No. eaaw2399.
- (55) Weeks, J. D.; Chandler, D.; Andersen, H. C. Role of Repulsive Forces in Determining the Equilibrium Structure of Simple Liquids. *J. Chem. Phys.* **1971**, 54 (12), 5237–5247.
- (56) Plimpton, S. Fast Parallel Algorithms for Short-Range Molecular Dynamics. *J. Comput. Phys.* **1995**, *117* (1), 1–19.